Kinetic Mechanism of Ligand Binding in Human Ileal Bile Acid Binding Protein as Determined by Stopped-Flow Fluorescence Analysis †

ARTICLE *in* BIOCHEMISTRY · JUNE 2007

Impact Factor: 3.02 · DOI: 10.1021/bi700030r · Source: PubMed

3 AUTHORS:

Orsolya Toke
Hungarian Academy of Sciences
20 PUBLICATIONS **481** CITATIONS
SEE PROFILE

John Monsey
Washington University in St. Louis
10 PUBLICATIONS **315** CITATIONS
SEE PROFILE

David Cistola
University of North Texas HSC at Fort Worth
68 PUBLICATIONS **2,940** CITATIONS
SEE PROFILE

Kinetic Mechanism of Ligand Binding in Human Ileal Bile Acid Binding Protein as Determined by Stopped-Flow Fluorescence Analysis†

Orsolya Toke,*,‡,§ John D. Monsey,‡ and David P. Cistola*,‡

Department of Biochemistry and Molecular Biophysics, Washington University School of Medicine, St. Louis, Missouri 63110, and Institute of Structural Chemistry, Chemical Research Center, Hungarian Academy of Sciences, Budapest, Hungary

Received January 7, 2007; Revised Manuscript Received March 7, 2007

ABSTRACT: Cooperative ligand binding to human ileal bile acid binding protein (I-BABP) was studied using the stopped-flow fluorescence technique. The kinetic data obtained for wild-type protein are in agreement with a four-step mechanism where after a fast conformational change on the millisecond time scale, the ligands bind in a sequential manner, followed by another, slow conformational change on the time scale of seconds. This last step is more pronounced in the case of glycocholate (GCA), the bile salt that binds with high positive cooperativity and is absent in mutant I-BABP proteins that lack positive cooperativity in their bile salt binding. These results suggest that positive cooperativity in human I-BABP is related to a slow conformational change of the protein, which occurs after the second binding step. Analogous to that in the intestinal fatty acid binding protein (I-FABP), we hypothesize that ligand binding in I-BABP is linked to a disorder−order transition between an open and a closed form of the protein.

Human ileal bile acid binding protein (I-BABP[1]) is a member of the intracellular lipid binding protein family, a group of small, approximately 15 kDa proteins that are thought to facilitate the cellular trafficking and metabolic regulation of fatty acids, retinoids, cholesterol, and bile salts (*1*, *2*). Human I-BABP is abundantly expressed in the absorptive enterocytes of the distal small intestine (*3*−*5*) and is thought to play a role in the enterohepatic circulation of bile salts (*6*).

We have previously shown that human I-BABP binds two molecules of glycocholate (GCA), the physiologically most abundant bile salt, with low intrinsic affinity but a high degree of positive cooperativity (*7*). Cooperativity in bile salt-I-BABP recognition was found to be governed by the pattern of steroid ring hydroxylation, rather than the presence and type of side-chain conjugation (*8*). In addition, human I-BABP has been found to exhibit a high degree of site selectivity in its interactions with GCA and glycochenodeoxycholate (GCDA) (Figure 1), the two primary bile salts in humans (*9*). According to our recent mutagenesis investigation, cooperativity and site-selectivity are not linked in the protein (*10*). On the basis of the first generation NMR structure of the ternary complex of human I-BABP with

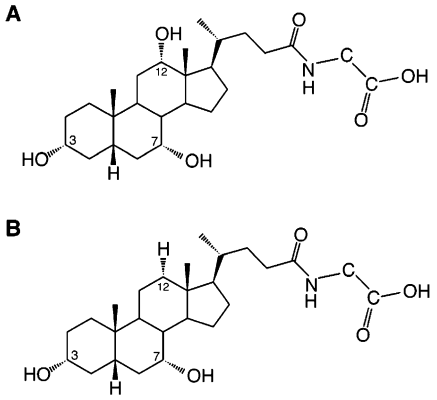

FIGURE 1: Chemical structures of glycocholic acid (GCA) (A) and glycochenodeoxycholic acid (GCDA) (B).

GCA and GCDA and the mutagenesis results (*10*), we postulated two cooperativity networks in the doubly ligated system: an upper network with the participation of residues N61 and W49 and a lower network with the participation of residues N61, E110 and possibly Q99. The upper network involves the steroid ring hydroxyl group at position C-12 (present only in GCA), whereas the lower network involves the steroid ring hydroxyl groups at positions C-3 and C-7 (present in both GCA and GCDA).

The purpose of the present study was to further investigate the bile acid binding properties of human I-BABP and to gain insight into the underlying mechanism of positive cooperativity in ligand binding. We employed the stopped-flow fluorescence technique to characterize the kinetics of binding in wild-type and various mutant I-BABPs that according to our previous thermodynamic study (*10*) exhibited diminished or no positive cooperativity. On the basis of kinetic observations, we conclude that wild-type human

† This work was supported by USPHS NIH grant R01 DK48046 to D.P.C. and by the Washington University Digestive Diseases Research Core Center, USPHFS NIH grant P30 DK52574.

* Corresponding author: Tel: 314-362-4382. Fax: 314-362-7183. E-mail: cistola@cosine.wustl.edu (D.P.C.). Tel: +36-1-438-4141/289. Fax: +36-1-325-7554. E-mail: toke@chemres.hu (O.T.).

‡ Washington University School of Medicine.

§ Hungarian Academy of Sciences.

[1] Abbreviations: GCA, glycocholic acid; GCDA, glycochenodeoxycholic acid; ITC, isothermal titration calorimetry; I-BABP, ileal bile acid-binding protein; I-FABP, intestinal fatty acid-binding protein; MPA, matrix projection algorithm; NMR, nuclear magnetic resonance; WT, wild type.

10.1021/bi700030r CCC: $37.00
Published on Web 04/14/2007

I-BABP undergoes a slow conformational change after both sites become occupied, a kinetic step that is missing in mutants that lack positive cooperativity.

MATERIALS AND METHODS

Sample Preparation. The methods used for biosynthesis and purification of wild-type and mutant human I-BABPs are detailed elsewhere (*10*). Protein was dialyzed into a buffer containing 20 mM potassium phosphate, 135 mM KCl, 10 mM NaCl, and 0.05% NaN_3 at pH 7.2. Protein concentrations were determined by absorbance at 280 nm. Extinction coefficients corresponding to a 1 mg/mL solution of the appropriate human I-BABP in water were obtained using composition analysis according to Pace et al. (*11*) and were as follows: wild type, 0.91; N61A, 0.851; Q99A, 0.876; and E110A, 0.869 A/mg/mL. Bile salts were obtained from Sigma (St. Louis, MO) and were dissolved in the same buffer to prepare stock solutions in the concentration range of 10 μM to 5 mM.

Stopped-Flow Fluorescence Spectroscopy. Kinetic measurements of bile salt binding to wild-type and various mutant human I-BABPs were performed using an Applied Photophysics stopped-flow spectrophotometer (model SX18MV). Changes in fluorescence ($\lambda_{excitation}$ = 290 nm; $\lambda_{emission}$ > 305 nm with an Oriel WG305 Schott glass filter and with excitation monochromator slits at 2 mm (band-pass ≈ 8 nm)) were followed at 25 °C in 20 mM potassium phosphate, 135 mM KCl, 10 mM NaCl, and 0.05% NaN_3 at pH 7.2. The protein, at a concentration of 2 μM, was mixed with an equal volume of GCA or GCDA in the same buffer so that the final bile salt concentrations ranged from 5 to 500 μM unless noted otherwise. At and below 500 μM, no self-association of bile salts was observed on the basis of light scattering. Under these conditions, the dead time of the stopped-flow instrument was less than ~2 ms (*12*). A total of 1000 points were collected in each trace. Usually, 7−8 individual traces were averaged at each set of conditions. The kinetic curves were fitted to extract the observed rates and amplitudes using the nonlinear least-squares software provided by the manufacturer, with a single or a sum of exponential functions defined as

$$F(t) = F_\infty + \sum_{i=1}^{n} A_i \exp(-\zeta_i t) \quad (1)$$

where $F(t)$ is the fluorescence intensity at time t, $F(\infty)$ is the fluorescence intensity at $t = \infty$, and ζ_i is the observed rate of the ith kinetic process occurring with an amplitude A_i. Kinetic simulations and all further analysis of the data were performed with Dynafit (*13*) and Mathematica (Wolfram, Urbana, IL).

RESULTS

Ligand Binding Kinetics to Wild-Type Human I-BABP. Stopped-flow fluorescence experiments were used to gain insight into the kinetic mechanism of bile salt binding in human I-BABP. The experiments have been performed under pseudo-first-order conditions by mixing the protein with an excess of ligand. Stopped-flow traces showing fluorescence changes upon GCA and GCDA binding to wild-type human I-BABP are shown in Figure 2. For GCDA, the first binding step is accompanied by a well-noticeable negative fluorescence change. In the case of GCA, because of the strong positive cooperativity of the system, the population of the singly ligated protein is small, and the existence of the quenching step was only confirmed after the full analysis of the data set.

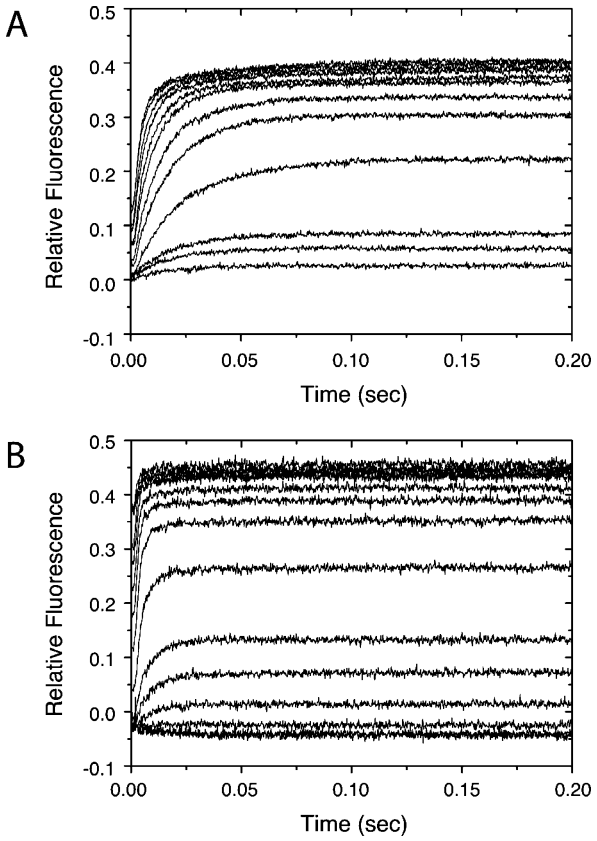

FIGURE 2: Stopped-flow traces showing fluorescence changes upon mixing human I-BABP with (A) GCA and (B) GCDA in buffer containing 20 mM potassium phosphate, 135 mM KCl, 10 mM NaCl, and 0.05% NaN_3 at pH 7.2 and 25 °C (λ_{ex} = 290 nm, λ_{em} > 305 nm). Final protein concentration was 1 μM. Final bile salt concentrations were as follows: GCA, 30, 40, 50, 100, 150, 200, 250, 300, 350, 400, 450, and 500 μM; GCDA, 5, 10, 20, 30, 40, 50, 100, 150, 200, 250, 300, 350, 400, 450, and 500 μM.

Representative traces at low and high ligand concentrations fitted with single and double exponentials are shown in Figure 3. It is evident that single exponentials failed to give adequate fitting of the data, particularly at higher ligand concentrations and particularly for GCA. Inclusion of a third exponential did not further improve the quality of the fits for either bile salt at 25 °C.

The observed rates obtained from biexponential fits are shown in Figure 4. For both GCA and GCDA, one of the rates ($k_{app,1}$) first decreases and then increases with increasing bile salt concentration. This behavior is expected for a multistep binding process, for which the eigenvalues (observed rates) can be given in terms of a quadratic or higher order function of the ligand concentration. At higher [L], the dependence of the observed rate on [L] is close to linear and the rate(s) of association can be estimated from the slope of the curve. For both bile salts, the rate constant of association in the first binding step is near 1 $\mu M^{-1}\,s^{-1}$, which is well below the diffusion-controlled limit.

The other rate that we detected ($k_{app,2}$) shows no change (within experimental error) with GCA or GCDA concentra-

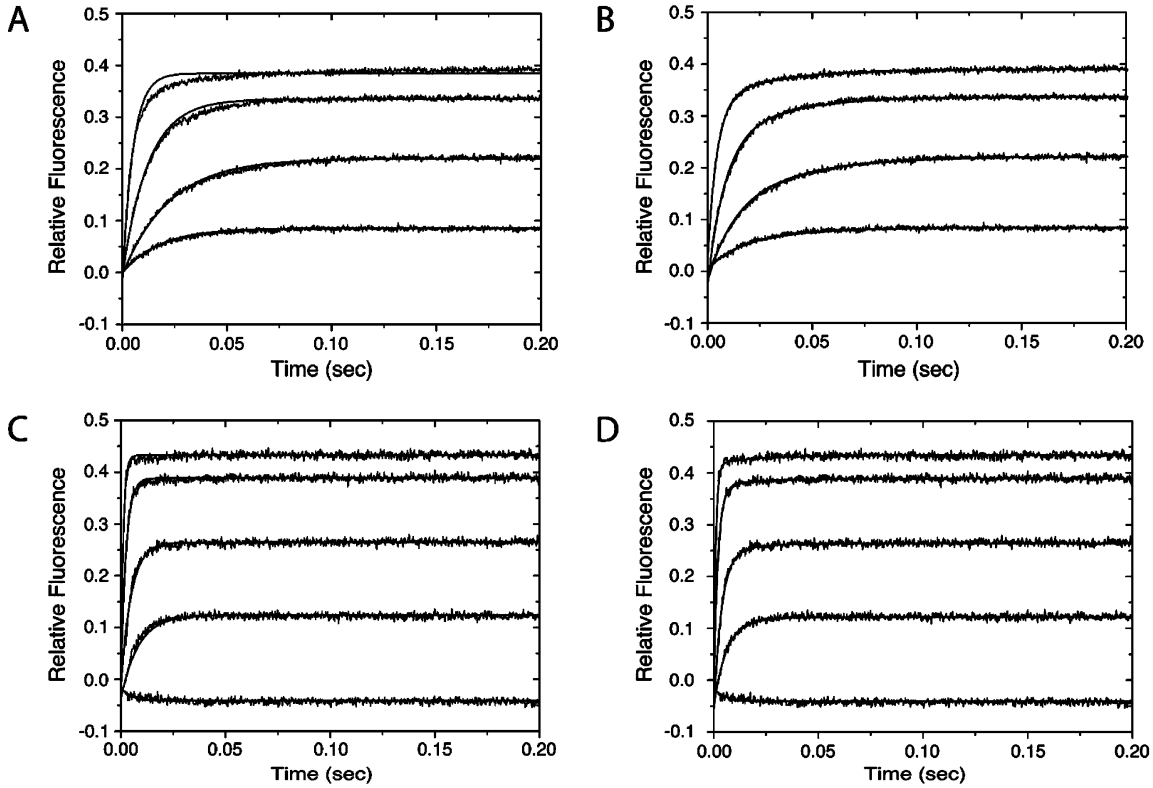

FIGURE 3: Representative stopped-flow traces from Figure 2 at different bile salt concentrations (GCA, top: 50, 100, 200, and 400 μM; GCDA, bottom: 10, 50, 100, 200, and 400 μM) and their nonlinear least-squares fits using a single (A and C) or a double (B and D) exponential according to eq 1.

tion, suggesting the existence of a unimolecular process in the binding mechanism. Although the amplitude of the exponential associated with the bimolecular step was about the same for both bile salts, the amplitude of the exponential associated with the unimolecular step was about an order of magnitude larger for GCA, the bile salt that binds with higher positive cooperativity (Hill coefficient of 1.82 (GCA) vs 1.34 (GCDA) at 25 °C (*8*)).

To summarize our observations so far, we detected (i) one of the two association steps and (ii) a slow unimolecular step, most likely a conformational change. On the basis of these observations, there are two possibilities: a slow conformational change occurring either between the two binding steps (Figure 5, Scheme I) or after the second binding step (Figure 5, Scheme II). The most elegant way to distinguish between these two possibilities would be to perform two sets of stopped-flow experiments: one under pseudo-first-order conditions with respect to the ligand and another one under pseudo-first-order conditions with respect to the macromolecule (*14*). In our system, the latter, unfortunately, was not possible because of the small signal change at low ligand-to-macromolecule molar ratios. However, in the case of GCA, Scheme I (Figure 5) gave poor fits to stopped-flow traces above 250 μM final bile salt concentration, suggesting that the slow unimolecular step occurs after the second binding step. This was later on confirmed by fitting of the extracted observed rates and amplitudes (cf. below).

That the association rate of the first binding step is well below the diffusion-controlled limit for both bile salts suggests the existence of a rate-limiting kinetic step in the binding mechanism. From a previous investigation of lipid binding proteins with the same topology (i.e., intestinal fatty acid binding protein (I-FABP)), we learned that prior to binding, the protein undergoes a conformational change on the millisecond time scale that allows the ligand to enter into the binding cavity (*15*, *16*). Above 1 mM final bile salt concentration, we saw $k_{app,1}$ reaching a similar plateau in I-BABP as well, but this was already in the concentration range where self-association of bile salts may take place. Also, the apparent rates at such high ligand concentration were already too fast to be accurately determined with our instrument. Nevertheless, the possibility of a fast conformational change prior to the binding of the first ligand had to be considered. To investigate this possibility, we incorporated a fast conformational change into the binding model (Figure 5, Scheme III), which slightly improved the quality of the fits but had no effect on the value of the rate constants for the subsequent steps, indicating that this conformational change, if it exists in wild-type I-BABP, is shifted to the right. Using $k_{app,1}$ as a lower limit for k_1 in Scheme III (Figure 5), a grid of k_1 and k_{-1} values has been constructed and tested with Dynafit. The best results were obtained with $\sim$1600 and $\sim$100 s^{-1} for the forward and reverse rate constants, respectively.

Dynafit also provided good estimates of the rate constants and fluorescence response factors associated with the subsequent steps. These were used as initial values in the computer fits of the observed rates. The solid lines in Figure 4 are least-square fits of the two observed rates according to the mechanism depicted in Scheme III (Figure 5). Observed rates were calculated as eigenvalues of coefficient matrices as a function of ligand concentration using Mathematica. The obtained rate constants for GCA and GCDA

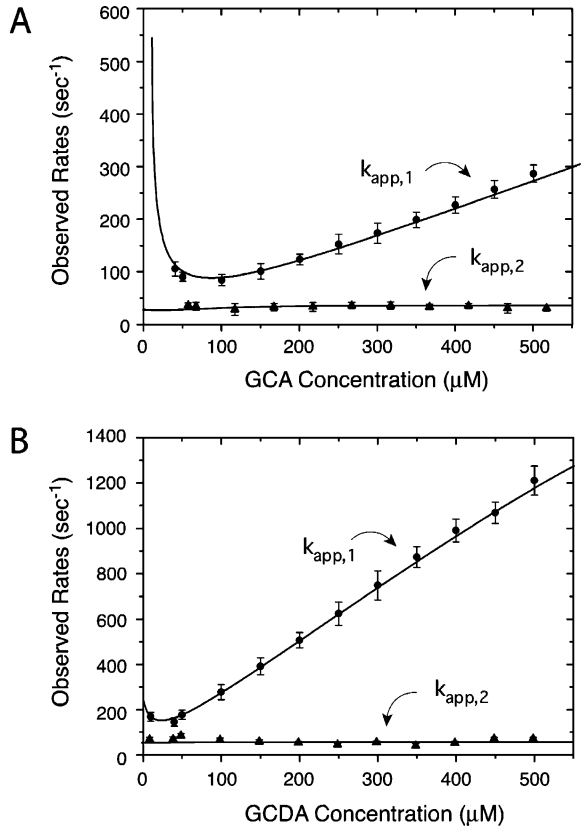

FIGURE 4: Observed rates for the binding of (A) GCA and (B) GCDA to human I-BABP as a function of ligand concentration as determined from the stopped-flow experiments (20 mM potassium phosphate, 135 mM KCl, 10 mM NaCl, and 0.05% NaN_3 at pH 7.2 and 25 °C). The solid lines are nonlinear least-square fits according to the four-step sequential mechanism defined in Scheme III (Figure 5), with rate constants $k_1 = 1600\ s^{-1}$, $k_{-1} = 100\ s^{-1}$, $k_2 = 0.58\ \mu M^{-1}\ s^{-1}$, $k_{-2} = 597\ s^{-1}$, $k_3 = 83\ \mu M^{-1}\ s^{-1}$, $k_{-3} = 536\ s^{-1}$, $k_4 = 7.9\ s^{-1}$, $k_{-4} = 27\ s^{-1}$ for the binding of GCA and $k_1 = 1600\ s^{-1}$, $k_{-1} = 100\ s^{-1}$, $k_2 = 2.68\ \mu M^{-1}\ s^{-1}$, $k_{-2} = 259\ s^{-1}$, $k_3 = 32\ \mu M^{-1}\ s^{-1}$, $k_{-3} = 554\ s^{-1}$, $k_4 = 2.3\ s^{-1}$, $k_{-4} = 50\ s^{-1}$ for the binding of GCDA (Table 1).

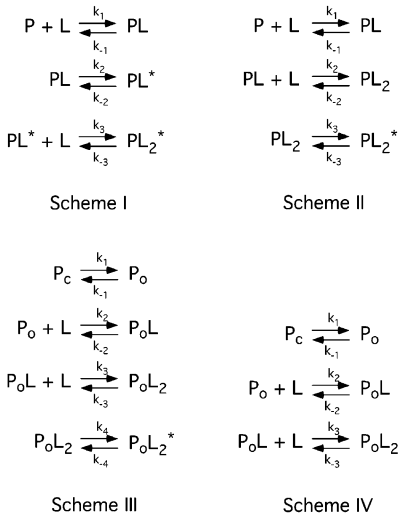

FIGURE 5: Schemes showing the kinetic mechanisms considered for bile salt binding to human I-BABP.

are shown in Table 1. Dissociation constants for the two binding steps can be calculated in terms of the rate constants and are also included in Table 1. They are in good agreement with the dissociation constants we previously determined from an ITC analysis of bile salt binding to human I-BABP (*10*).

Table 1: Kinetic, Thermodynamic and Spectroscopic Parameters Characterizing the Binding of GCA and GCDA to Wild-Type Human I-BABP According to the Mechanism in Scheme III (Figure 5)[a]

	GCA	GCDA
k_1 (s^{-1})	1600 ± 300	1600 ± 300
k_{-1} (s^{-1})	100 ± 50	100 ± 50
k_2 ($\mu M^{-1}\ s^{-1}$)	0.58 ± 0.04	2.68 ± 0.08
k_{-2} (s^{-1})	597 ± 28	259 ± 9
k_3($\mu M^{-1}\ s^{-1}$)	83 ± 12	32 ± 1
k_{-3} (s^{-1})	536 ± 43	554 ± 22
k_4 (s^{-1})	7.9 ± 0.3	2.3 ± 0.4
k_{-4} (s^{-1})	27 ± 3	50 ± 6
K_{d1} (μM, this study)	1094 ± 118	103 ± 11
K_{d1} (μM, ITC)[b]	748 ± 170	103 ± 5
K_{d2} (μM, this study)	5 ± 1	17 ± 4
K_{d2} (μM, ITC)[b]	5.9 ± 1.1	26 ± 1
ΔF_2	0	0
ΔF_3	−1.27 ± 0.18	−0.83 ± 0.36
ΔF_4	0.38 ± 0.08	0.54 ± 0.25
ΔF_5	0.58 ± 0.12	0.93 ± 1.4

[a] Buffer conditions: 20 mM potassium phosphate, 135 mM KCl, 10 mM NaCl, and 0.05% NaN_3 at pH 7.2 and 25 °C. [b] From ref 10 (*10*).

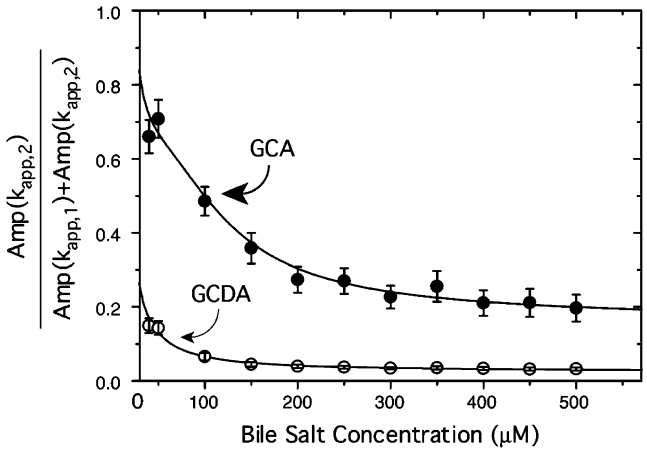

FIGURE 6: Normalized amplitude of the slow, unimolecular step as a function of ligand concentration as determined from the stopped-flow experiments (20 mM potassium phosphate, 135 mM KCl, 10 mM NaCl, and 0.05% NaN_3 at pH 7.2 and 25 °C). The solid lines are nonlinear least-square fits according to eq A15 describing the four-step sequential mechanism defined in Scheme III (Figure 5) with rate constants and relative fluorescence intensities shown in Table 1.

The obtained rate constants were then used in the fitting of the amplitudes associated with the two observed rates. This was accomplished using the matrix projection operator technique (*17*, *18*), a method that allows us to determine the molar fluorescence intensities corresponding to the various macromolecular species in the reaction (Appendix). The solid lines in Figure 6 are least-square fits of the observed normalized amplitudes associated with the slow, unimolecular step ($k_{app,2}$) according to the mechanism shown in Scheme III (Figure 5). The obtained relative molar fluorescence parameters are shown in Table 1.

The resulting rate constants and fluorescence response factors provide good fits of the stopped-flow traces for both bile salts. This is demonstrated in Figure 7, where fits

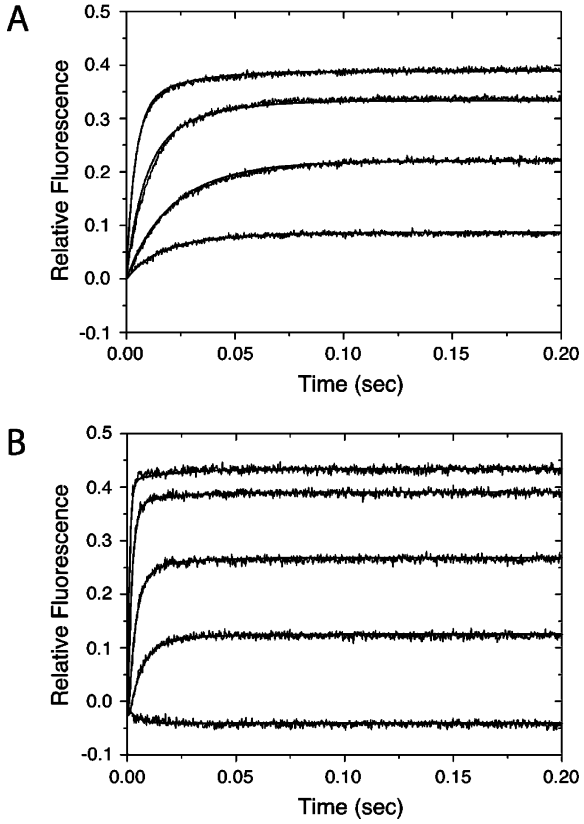

FIGURE 7: Representative stopped-flow traces from Figure 2 at different final bile salt concentrations ((A) GCA: 50, 100, 200, and 400 μM; (B) GCDA: 10, 50, 100, 200, and 400 μM) and their nonlinear least-squares fits obtained with the matrix projection operator technique according to eq A12.

obtained with the matrix projection operator technique are shown at various GCA and GCDA concentrations.

Ligand Binding Kinetics to Various Human I-BABP Mutants. To further investigate whether the observed slow unimolecular step is indeed related to positive binding cooperativity in the protein, we investigated the kinetics of bile salt binding to various mutant human I-BABPs (Figure 8). Previously, we have shown that mutations to alanine at residues N61, Q99, and E110 resulted in a complete loss of positive cooperativity for the binding of GCDA (*10*). Mutation at residue N61 severely diminished the cooperativity of the binding of GCA as well. Representative stopped-flow traces showing fluorescence changes upon GCDA binding under pseudo-first-order conditions to mutants N61A, Q99A, and E110A human I-BABP are shown in Figure 9. Interestingly, the signal changes are significantly smaller for all three mutants compared to those for the wild-type protein, indicating that the tryptophan residue (W49, located in the middle of the binding pocket in wild-type hI-BABP), has become a less sensitive fluorescence marker of ligand binding. Because of the loss of positive cooperativity, the two binding steps are decoupled in these mutants, and the fluorescence decrease in the first step and the enhancement in the second step (Q99A and E110A) are more apparent than those in wild-type human I-BABP. In mutant N61A, both binding steps result in an enhancement of the fluorescence signal. The solid lines in Figure 9 are single exponentials used for fitting of the stopped-flow traces. Unlike in wild-type protein (Figure 3), the inclusion of a second exponential in the fitting equation did not improve

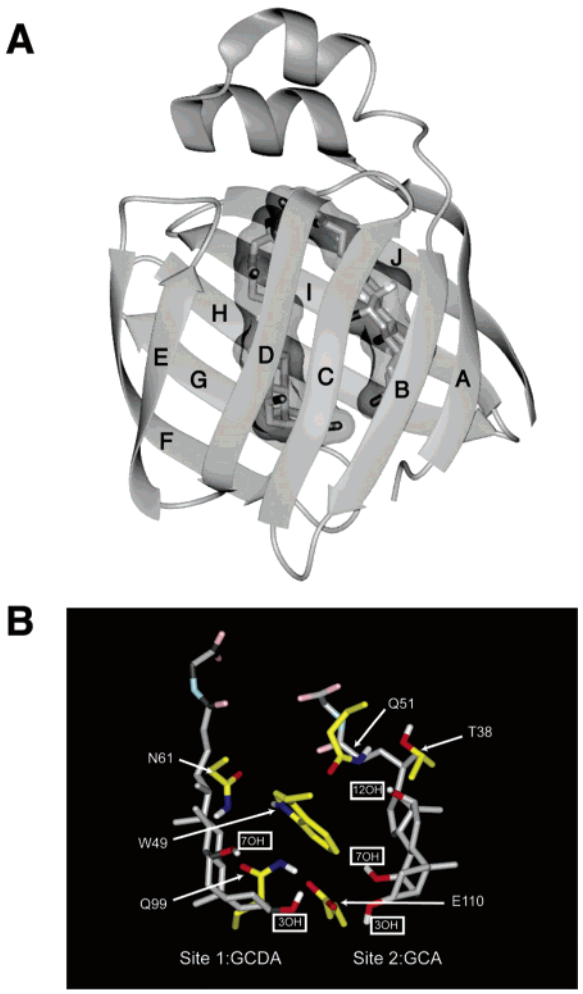

FIGURE 8: Homology model of human I-BABP with GCA and GCDA docked by restrained energy minimization. (A) Human I-BABP binds two molecules of bile salts in an enclosed cavity surrounded by two antiparallel β-sheets. (B) The binding pocket of human I-BABP showing various key residues identified by mutagenesis. This Figure was adapted from ref 10 (*10*).

the quality of fits any further. The observed rates for the binding of GCDA obtained from single-exponential fits for mutant N61A, Q99A, and E110A I-BABP are shown in Figure 10. For these I-BABP derivatives, the rates plateau near 1300, 800, and 350 s^{-1}, respectively, indicating the existence of a rate-limiting kinetic step on the millisecond time scale. This is analogous to our observations in I-FABP and provides a support to the kinetic mechanism depicted in Scheme III (Figure 5) for wild-type I-BABP.

In the absence of the slow unimolecular step observed for wild-type protein, for mutants N61A, Q99A, and E110A we propose a three-step binding mechanism according to Scheme IV (Figure 5). Rate constants and relative molar fluorescence parameters have been determined with Dynafit and are shown in Table 2.

DISCUSSION

Cooperative binding processes are frequent in biological systems. Cooperativity has implications for the regulation of enzymes and receptors, thereby maintaining a stable, nontoxic internal environment in living organisms. For instance, in the case of human I-BABP, with the relatively low intrinsic affinities of the protein for both GCA and

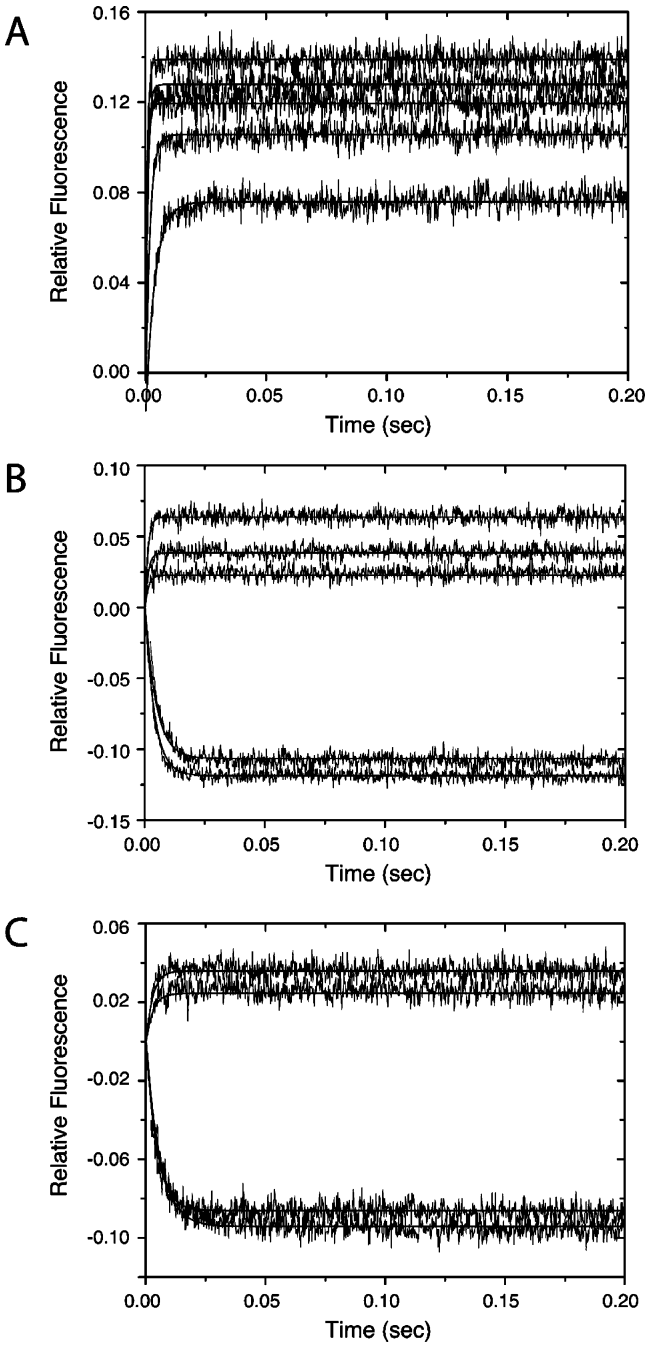

FIGURE 9: Representative stopped-flow traces showing fluorescence changes upon GCDA binding to mutants (A) N61A, (B) Q99A, and (C) E110A human I-BABP in buffer containing 20 mM potassium phosphate, 135 mM KCl, 10 mM NaCl, 0.05% NaN_3 at pH 7.2 and 25 °C ($\lambda_{ex} = 290$ nm; $\lambda_{em} > 305$ nm). The final protein concentration was 1 μM in each experiment. Final GCDA concentrations were 20, 40, 250, 300, and 400 μM for N61A; 40, 80, 250, 300, and 400 μM for Q99A; and 20, 40, 300, and 400 μM for E110A. The solid lines are nonlinear least-square fits to the data using a single exponential according to eq 1.

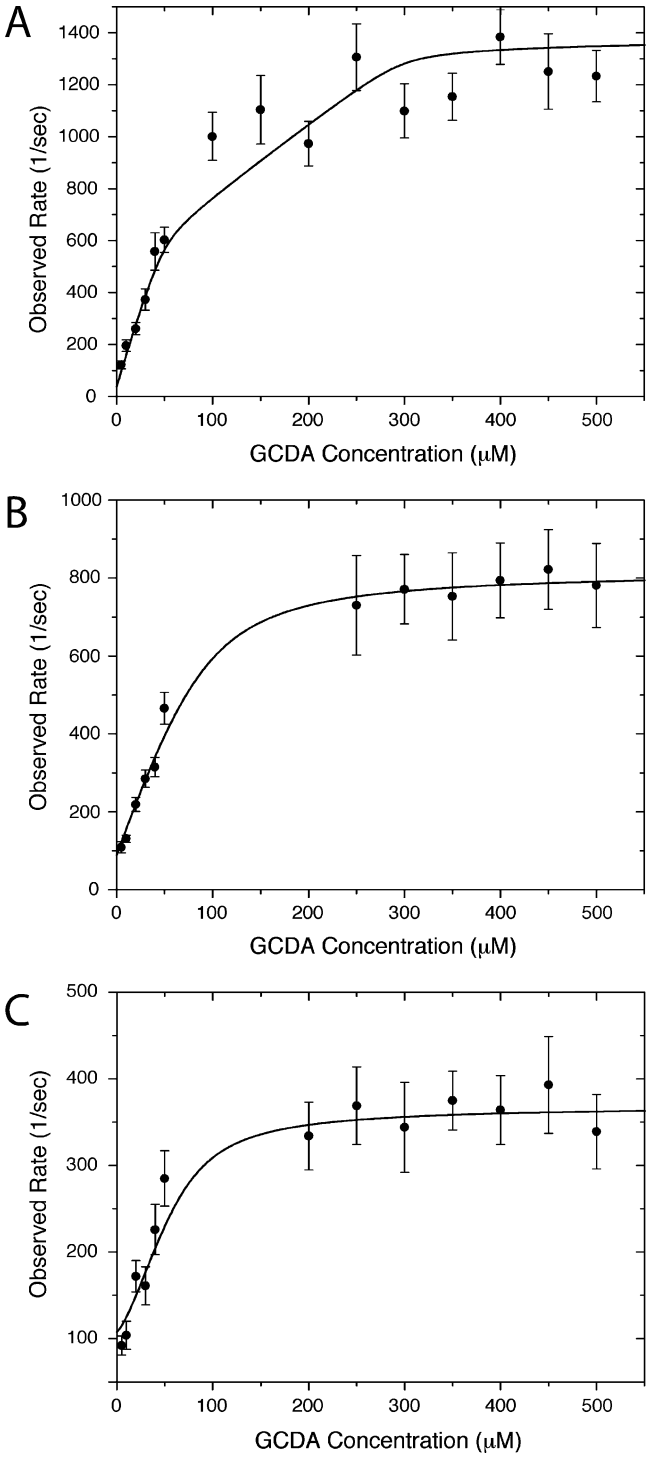

FIGURE 10: Observed rates for the binding of GCDA to (A) N61A, (B) Q99A, and (C) E110A human I-BABP as a function of ligand concentration as determined from the stopped-flow experiments (20 mM potassium phosphate, 135 mM KCl, 10 mM NaCl, and 0.05% NaN_3 at pH 7.2 and 25 °C). The solid lines are nonlinear least-square fits according to the three-step sequential mechanism defined in Scheme IV (Figure 5), with the rate constants listed in Table 2.

GCDA (*7*), positive cooperativity allows a sizable fraction of bile salts to remain unbound at low bile salt concentration (passing through the enterocytes as monomers), whereas protecting the cells from bile salt toxicity (e.g., apoptosis (*19*)) at high bile salt concentrations.

Although binding cooperativity is most often associated with proteins that possess multiple subunits, there are a number of examples among monomeric proteins as well. The list includes the Ca^{2+}-binding protein, calbindin D_{9k} (*20*), the binding of glucose to glucokinase (*21*), and the pH dependence of ion transport through the mitochondrial VDAC (voltage-dependent anion channel) channel (*22*).

In theory, there can be two possible explanations for cooperativity. One possibility is that the binding of the first

Table 2: Kinetic, Thermodynamic and Spectroscopic Parameters Characterizing the Binding of GCDA to Various Human I-BABP Mutants According to the Mechanism in Scheme IV (Figure 5)[a]

	N61A	Q99A	E110A
k_1 (s^{-1})	1400 ± 270	820 ± 140	370 ± 110
k_{-1} (s^{-1})	150 ± 40	140 ± 36	50 ± 25
k_2 (μM^{-1} s^{-1})	14 ± 0.7	8.8 ± 0.2	5.4 ± 0.1
k_{-2} (s^{-1})	38 ± 5	89 ± 11	108 ± 18
k_3 (μM^{-1} s^{-1})	2.8 ± 0.4	11 ± 0.3	11.6 ± 0.9
k_{-3} (s^{-1})	509 ± 46	1650 ± 160	463 ± 55
K_{d1} (μM, this study)	3 ± 1	12 ± 2	23 ± 6
K_{d1} (μM, ITC)[b]	44 ± 1	13 ± 1	48 ± 1
K_{d2} (μM, this study)	182 ± 26	150 ± 17	40 ± 9
K_{d2} (μM, ITC)[b]	401 ± 10	142 ± 10	41 ± 1
ΔF_2	0	0.184 ± 0.07	0
ΔF_3	0.08 ± 0.02	−0.28 ± 0.05	−0.33 ± 0.09
ΔF_4	0.16 ± 0.03	0.20 ± 0.02	0.07 ± 0.01

[a] The parameters obtained for the wild-type protein are shown in Table 1. Buffer conditions: 20 mM potassium phosphate, 135 mM KCl, 10 mM NaCl, and 0.05% NaN_3 at pH 7.2 and 25 °C. [b] From ref 10 (*10*).

ligand provides a favorable binding surface for the second through a direct ligand−ligand interaction. Alternatively, cooperativity could result from allostery, where bile salt binding is energetically linked to a conformational change in the protein.

In our investigation of human I-BABP, we used stopped-flow spectrofluorometry to gain insight into the kinetic mechanism of bile salt binding. The kinetic data we obtained for the wild-type protein fit best to a reversible four-step model shown in Scheme III (Figure 5). According to this model, after a fast conformational change on the millisecond time scale (opening step), the ligands bind in a sequential manner, followed by another, slow conformational change on the time scale of seconds. This last step is more pronounced in the case of GCA, the bile salt that binds with high positive cooperativity and is absent in mutant I-BABP proteins that lack positive cooperativity in their bile salt binding. These results suggest that positive cooperativity in human I-BABP is related to a slow conformational change of the protein, which occurs after the second binding step. This transition into a lower energy conformation after the binding of the second bile salt molecule is also supported by the large enthalpically favorable contribution to the overall free energy change that accompanies the second binding step (*8*, *10*).

GCA and GCDA: Subtle Difference in Structure Results in Strikingly Different Binding Properties. Although GCA and GCDA differ only in a single OH group at position C-12 of their steroid ring system (Figure 1), the strength of their binding cooperativity is remarkably different. Previously, we have also shown that the binding of these two bile salts is site-selective, and site selectivity mainly arises from the strong intrinsic affinity of GCDA for site 1.

According to the kinetic data we obtained from the stopped-flow analysis, although the dissociation rate constant is similar, the association rate constant for the first binding step is about five times faster for GCDA than for GCA (Table 1). The difference between the association and the dissociation rate of the first binding step is further diminished in mutant I-BABP proteins that lack positive cooperativity (Table 2). The selective increase in the association rate of

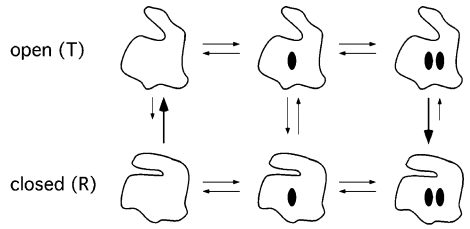

FIGURE 11: Allosteric model for the binding of bile salts to human I-BABP. *See text for details.*

GCDA in the first binding step, which is likely related to the strong affinity of GCDA for site 1, in the end results in a smaller positive cooperativity for this bile salt. Regarding the second binding step, the association and dissociation steps are similar for GCA and GCDA. Finally, the interconversion between P_oL_2 and $P_oL_2^*$ in the subsequent unimolecular step is slow for both bile salts ($k_4 = 7.9$ s^{-1}, $k_{-4} = 27$ s^{-1} for GCA and $k_4 = 2.3$ s^{-1}, $k_{-4} = 50$ s^{-1} for GCDA), indicating a large kinetic energy barrier between the two conformations. The relative amplitude of this step in comparison with that of the first bimolecular step is about 10-fold higher for GCA, the bile salt exhibiting high positive cooperativity.

Interactions Responsible for Positive Binding Cooperativity in Human I-BABP. Generally, the energy of positive cooperativity may result from two sources: enthalpically favorable interactions (electrostatic, H-bond, and van der Waals) as well as entropically favorable changes related to molecular flexibility and disorder.

Positive binding cooperativity in wild-type human I-BABP can be explained in terms of a modified Monod−Wyman−Changeux model (*23*) as shown in Figure 11. According to this scheme, there are two distinct conformational states of the protein: an open (T) state and a closed (R) state, in which T is thermodynamically favored in the absence of ligands, but upon ligand binding, the equilibrium is shifted toward the R state. This transition between the open and closed forms of the protein is realized after the occupation of both binding sites and is a result of the stronger affinity of the R state for the ligands. The stronger affinity of R may originate from various local and long-range interactions in the protein−ligand complex. Specifically, the portal region of I-BABP may become more stable by ligand binding, as we proposed earlier for I-FABP, another lipid binding protein with the same topology (*16*). According to the dynamic portal hypothesis, I-FABP exists as a manifold of locally ordered and disordered states in solution, and a localized region of backbone disorder is part of a flexible portal that permits the entry of ligand. Fatty acid binding shifts the order−disorder equilibrium toward the ordered, closed state by stabilizing a series of interactions between helix II and the C−D turn of the protein. Strands C, D, and the turn between them in I-BABP surround half of the binding cavity, containing residues W49 and N61 (Figure 8). Mutations at these residues result in losses of positive binding cooperativity supporting the notion that these residues are part of a H-bonding network in the protein−bile salt complex that connects the two sites. Another residue, residue Q51 at the end of strand C has been found to play a role in the site selectivity of bile salt binding. Moreover, on the basis of the fluorescence response factors determined from the

stopped-flow analysis, besides the formation of H-bonds between bile salts and certain donor/acceptor residues in the binding pocket, the burial of hydrophobic side chains such as the side chain of W49 likely contributes to the energy of positive cooperativity in the protein. We note that a number of additional bile salt−amino acid contacts have been determined in this region of the protein by NMR including contacts with residues Y53 and F63 (data not shown). Thus, it seems plausible that similar to fatty acid binding to I-FABP, bile salt binding to I-BABP induces a conformational change in this region of the protein that in addition to the local effects may have implications for the long-range interactions with the portal region as well.

The disorder−order transition between the open and closed forms of I-BABP is based on the unexpectedly slow (∼1 μM^{-1} s^{-1}) association rate constant of the first binding step, the rate-limiting conformational change on the millisecond time scale we observed in some of the I-BABP derivatives, the large entropically unfavorable change that accompanies the second binding step (*8*), and the analogy with I-FABP. NMR relaxation studies directed at the backbone and side-chain dynamics of human I-BABP complexes should give more insight into the role of dynamics in the cooperative nature of the system (*24*, *25*).

ACKNOWLEDGMENT

We are indebted to Dr. Carl Frieden for generously providing the instrument for the stopped-flow analysis and for helpful discussions on the manuscript.

APPENDIX

The differential equations describing the time course of the reaction written in Scheme III (Figure 5) are as follows:

$$\frac{d[P_c]}{dt} = -k_1[P_c] + k_{-1}[P_o]$$

$$\frac{d[P_o]}{dt} = k_1[P_c] - k_{-1}[P_o] - k_2[P_o][L] + k_{-2}[P_oL]$$

$$\frac{d[P_oL]}{dt} = k_2[P_o][L] - k_{-2}[P_oL] - k_3[P_oL][L] + k_{-3}[P_oL_2]$$

$$\frac{d[P_oL_2]}{dt} = k_3[P_oL][L] - k_{-3}[P_oL_2] - k_4[P_oL_2] + k_{-4}[P_oL_2{}^*]$$

$$\frac{d[P_oL_2{}^*]}{dt} = k_4[P_oL_2] - k_{-4}[P_oL_2{}^*] \quad \text{(A1)}$$

The stopped-flow experiments described in this study have been performed under pseudo-first-order conditions with a large excess of the bile salt over the protein, $[L_{tot}] \gg [P_{tot}]$. Therefore, the concentration of the free ligand, [L], can be approximated with $[L_{tot}]$ during the reaction. In matrix notation, the system is defined as follows:

$$\begin{pmatrix} \frac{d[P_c]}{dt} \\ \frac{d[P_o]}{dt} \\ \frac{d[P_oL]}{dt} \\ \frac{d[P_oL_2]}{dt} \\ \frac{d[P_oL_2{}^*]}{dt} \end{pmatrix} = \begin{pmatrix} -k_1 & k_{-1} & 0 & 0 & 0 \\ k_1 & -k_{-1} - k_2[L_{tot}] & k_{-2} & 0 & 0 \\ 0 & k_2[L_{tot}] & -k_{-2} - k_3[L_{tot}] & k_{-3} & 0 \\ 0 & 0 & k_3[L_{tot}] & -k_{-3} - k_4 & k_{-4} \\ 0 & 0 & 0 & k_4 & -k_{-4} \end{pmatrix} \begin{pmatrix} [P_c] \\ [P_o] \\ [P_oL] \\ [PoL_2] \\ [P_oL_2{}^*] \end{pmatrix} \quad \text{(A2)}$$

or

$$\dot{\mathbf{N}} = \mathbf{M}\mathbf{N} \quad \text{(A3)}$$

where **N** is the vector of concentrations of different I-BABP species in solution, $\dot{\mathbf{N}}$ is the vector of time derivatives of these concentrations, and **M** is the coefficient matrix. The solution of eq A3 can be written as follows:

$$\mathbf{N} = \exp(\mathbf{M}t)\mathbf{N}_0 \quad \text{(A4)}$$

where

$$\exp(\mathbf{M}t) = \mathbf{V} \begin{pmatrix} \exp(\zeta_0 t) & 0 & 0 & 0 & 0 \\ 0 & \exp(\zeta_1 t) & 0 & 0 & 0 \\ 0 & 0 & \exp(\zeta_2 t) & 0 & 0 \\ 0 & 0 & 0 & \exp(\zeta_3 t) & 0 \\ 0 & 0 & 0 & 0 & \exp(\zeta_4 t) \end{pmatrix} \mathbf{V}^{-1} \quad \text{(A5)}$$

Quantities ζ_0, ζ_1, ζ_2, ζ_3, and ζ_4 are the eigenvalues of matrix **M**, **V** is a matrix whose columns are the eigenvectors of matrix **M**, and $\mathbf{N_0}$ is the vector of initial concentrations of the various protein species. For the stopped-flow experiments described in this work, $\mathbf{N_0}$ is a column vector of (N_{tot}, 0, 0, 0, 0), where N_{tot} is the total concentration of the protein (1 μM). Matrix exp(**M**t) can be expanded using its eigenvalues, exp(ζ_it), and the corresponding projection operators, $\mathbf{Q_i}$, (*17*, *26*) as follows:

$$\exp(\mathbf{M}t) = \sum_{\mathbf{i=0}}^{\mathbf{4}} \mathbf{Q_i} \exp(\zeta_i t) \quad \text{(A6)}$$

where the projection operators $\mathbf{Q_i}$ are defined in terms of the original coefficient matrix **M** and its eigenvalues (*17*, *26*) according to the following equation:

$$\mathbf{Q_i} = \frac{\prod_{j \neq i}^{4} (\mathbf{M} - \zeta_j \mathbf{I})}{\prod_{j \neq i}^{4} (\zeta_i - \zeta_j)} \quad \text{(A7)}$$

where **I** is the identity matrix.

The solution to the set of differential equations in A1 can be obtained by substituting eq A6 and A7 into eq A4

$$\mathbf{N} = \mathbf{Q_0N_0} + \mathbf{Q_1N_0}\exp(\zeta_1 t) + \mathbf{Q_2N_0}\exp(\zeta_2 t) + \mathbf{Q_3N_0}\exp(\zeta_3 t) + \mathbf{Q_4N_0}\exp(\zeta_4 t) \quad \text{(A8)}$$

or

$$\mathbf{N} = \mathbf{P_0} + \mathbf{P_1}\exp(\zeta_1 t) + \mathbf{P_2}\exp(\zeta_2 t) + \mathbf{P_3}\exp(\zeta_3 t) + \mathbf{P_4}\exp(\zeta_4 t) \quad \text{(A9)}$$

where $\mathbf{P_i}$ is the projection of the initial concentrations of $\mathbf{N_0}$ on the *i*th eigenvector of the coefficient matrix **M**. Thus,the time dependence of the various protein species in solution can be written as

$$\begin{pmatrix} N_1 \\ N_2 \\ N_3 \\ N_4 \\ N_5 \end{pmatrix} = \begin{pmatrix} P_{01} \\ P_{02} \\ P_{03} \\ P_{04} \\ P_{05} \end{pmatrix} + \begin{pmatrix} P_{11} \\ P_{12} \\ P_{13} \\ P_{14} \\ P_{15} \end{pmatrix}\exp(\zeta_1 t) + \begin{pmatrix} P_{21} \\ P_{22} \\ P_{23} \\ P_{24} \\ P_{25} \end{pmatrix}\exp(\zeta_2 t) + \begin{pmatrix} P_{31} \\ P_{32} \\ P_{33} \\ P_{34} \\ P_{35} \end{pmatrix}\exp(\zeta_3 t) + \begin{pmatrix} P_{41} \\ P_{42} \\ P_{43} \\ P_{44} \\ P_{45} \end{pmatrix}\exp(\zeta_4 t) \quad \text{(A10)}$$

where P_{ij} is the *j*th element of the projection of $\mathbf{N_0}$ on the *i*th eigenvector of matrix **M**.

In the mechanism defined in Scheme III (Figure 5), one of the five eigenvalues, ζ_0 equals 0 because of the mass conservation of the reaction system. The four other eigenvalues of matrix **M** define the four observed rates of the reaction, $-\zeta_1$, $-\zeta_2$, $-\zeta_3$, and $-\zeta_4$. The individual amplitudes, A_1, A_2, A_3, and A_4, corresponding to these normal modes of the reaction, contain contributions from the fluorescence intensities of the various protein species present in solution. At any time of the reaction, the fluorescence of the system is defined as follows:

$$F(t) = F_1N_1 + F_2N_2 + F_3N_3 + F_4N_4 + F_5N_5 \quad \text{(A11)}$$

where F_1, F_2, F_3, F_4, and F_5 are the molar fluorescence intensities corresponding to macromolecular species N_1, N_2, N_3, N_4, and N_5. By substituting eq A10 into eq A11, we obtain the following

$$\begin{aligned} F(t) = {} & F_1(P_{01} + P_{11}\exp(\zeta_1 t) + P_{21}\exp(\zeta_2 t) + P_{31}\exp(\zeta_3 t) + P_{41}\exp(\zeta_4 t)) + F_2(P_{02} + P_{12}\exp(\zeta_1 t) + P_{22}\exp(\zeta_2 t) + P_{32}\exp(\zeta_3 t) + P_{42}\exp(\zeta_4 t)) + F_3(P_{03} + P_{13}\exp(\zeta_1 t) + P_{23}\exp(\zeta_2 t) + P_{33}\exp(\zeta_3 t) + P_{43}\exp(\zeta_4 t)) + F_4(P_{04} + P_{14}\exp(\zeta_1 t) + P_{24}\exp(\zeta_2 t) + P_{34}\exp(\zeta_3 t) + P_{44}\exp(\zeta_4 t)) + F_5(P_{05} + P_{15}\exp(\zeta_1 t) + P_{25}\exp(\zeta_2 t) + P_{35}\exp(\zeta_3 t) + P_{45}\exp(\zeta_4 t)) \end{aligned} \quad \text{(A12)}$$

The total amplitude, A_{tot}, of a stopped-flow trace is defined as

$$A_{tot} = F(\infty) - F(0) \quad \text{(A13)}$$

where $F(0)$ and $F(\infty)$ are the observed fluorescence intensities at $t = 0$ and $t = \infty$, respectively. The total amplitude is also the sum of the individual amplitudes corresponding to each normal mode of the reaction system.

$$A_{tot} = A_1 + A_2 + A_3 + A_4 \quad \text{(A14)}$$

With the combination of eqs A12, A13, and A14, the individual amplitudes can be given in terms of the projection matrix elements and the relative fluorescence intensities according to the following equations:

$$A_1 = (P_{12}\,P_{13}\,P_{14}\,P_{15})\begin{pmatrix} F_1 - F_2 \\ F_1 - F_3 \\ F_1 - F_4 \\ F_1 - F_5 \end{pmatrix} \quad \text{(A15a)}$$

$$A_2 = (P_{22}\,P_{23}\,P_{24}\,P_{25})\begin{pmatrix} F_1 - F_2 \\ F_1 - F_3 \\ F_1 - F_4 \\ F_1 - F_5 \end{pmatrix} \quad \text{(A15b)}$$

$$A_3 = (P_{32}\,P_{33}\,P_{34}\,P_{35})\begin{pmatrix} F_1 - F_2 \\ F_1 - F_3 \\ F_1 - F_4 \\ F_1 - F_5 \end{pmatrix} \quad \text{(A15c)}$$

$$A_4 = (P_{42}\,P_{43}\,P_{44}\,P_{45})\begin{pmatrix} F_1 - F_2 \\ F_1 - F_3 \\ F_1 - F_4 \\ F_1 - F_5 \end{pmatrix} \quad \text{(A15d)}$$

REFERENCES

1. Veerkamp, J. H., and Maatman, R. G. (1995) Cytoplasmic fatty acid-binding proteins: their structure and genes, *Prog. Lipid Res. 34*, 17−52.
2. Glatz, J. F., and van der Vusse, G. J. (1996) Cellular fatty acid-binding proteins: their function and physiological significance, *Prog. Lipid Res. 35*, 243−282.
3. Lin, M. C., Kramer, W., and Wilson, F. A. (1990) Identification of cytosolic and microsomal bile acid-binding proteins in rat ileal enterocytes, *J. Biol. Chem. 265*, 14986−14995.
4. Sacchettini, J. C., Hauft, S. M., van Camp, S. L., Cistola, D. P., and Gordon, J. I. (1990) Developmental and structural studies of an intracellular lipid binding protein expressed in the ileal epithelium, *J. Biol. Chem. 265*, 19199−19207.
5. Miller, K. R., and Cistola, D. P. (1993) Titration calorimetry as a binding assay for lipid-binding proteins, *Mol. Cell. Biochem. 123*, 29−37.
6. Small, D. M., Dowling, R. H., and Redinger, R. N. (1972) The enterohepatic circulation of bile salts, *Arch. Intern. Med. 130*, 552−573.
7. Tochtrop, G. P., Richter, K., Tang, C., Toner, J. J., Covey, D. F., and Cistola, D. P. (2002) Energetics by NMR: site-specific binding in a positively cooperative system, *Proc. Natl. Acad. Sci. U.S.A. 99*, 1847−1852.
8. Tochtrop, G. P., Bruns, J. M., Tang, C., Covey, D. F, and Cistola, D. P. (2003) Steroid ring hydroxylation patterns govern cooperativity in human bile acid binding protein, *Biochemistry 42*, 11561−11567.
9. Tochtrop, G. P., DeKoster, G. T., Covey, D. F., and Cistola, D. P. (2004) A single hydroxyl group governs ligand site selectivity in human ileal bile acid binding protein, *J. Am. Chem. Soc. 126*, 11024−11029.
10. Toke, O., Monsey, J. D., DeKoster, G. T., Tochtrop, G. P., Tang, C., and Cistola, D. P. (2006) Determinants of cooperativity and site-selectivity in human ileal bile acid-binding protein, *Biochemistry 45*, 727−737.
11. Pace, C. N., Vajdos, F., Fee, L., Grimsley, G., and Gray, T. (1995) How to measure and predict the molar absorption coefficient of a protein, *Protein Sci. 4*, 2411−2423.

12. Tonomura, B., Nakatani, H., Ohnishi, M., Yamaguchi-Ito, J., and Hiromi, K. (1978) Test reactions for a stopped-flow apparatus. Reduction of 2,6-dichlorophenolindophenol and potassium ferricyanide by L-ascorbic acid, *Anal. Biochem. 84*, 370−383.
13. Kuzmic, P. (1996) Program DYNAFIT for the analysis of enzyme kinetic data: application to HIV proteinase, *Anal. Biochem. 237*, 260−273.
14. Galletto, R., Jezewska, M. J., and Bujalowski, W. (2005) Kinetics of allosteric conformational transition of a macromolecule prior to ligand binding: analysis of stopped-flow kinetic experiments, *Cell. Biochem. Biophys*. *42*, 121−144.
15. Cistola, D. P., Kim, K., Rogl, H., and Frieden, C. (1996) Fatty acid interactions with a helix-less variant of intestinal fatty acid-binding protein, *Biochemistry 35*, 7559−7565.
16. Hodsdon, M. E., and Cistola, D. P. (1997) Discrete backbone disorder in the nuclear magnetic resonance structure of apo intestinal fatty acid-binding protein: implications for the mechanism of ligand entry, *Biochemistry 36*, 1450−1460.
17. Pilar, F. L. (1968) Introduction to Matrix Theory, in *Elementary Quantum Chemistry*, Chapter 9, McGraw-Hill, New York.
18. Bujalowski, W., and Jezewska, M. J. (2000) Kinetic mechanism of the single-stranded DNA recognition by *Escherichia coli* replicative helicase DnaB protein. Application of the matrix projection operator technique to analyze stopped-flow kinetics, *J. Mol. Biol. 295*, 831−852.
19. Pritchard, D. M., and Watson, A. J. (1996) Apoptosis and gastrointestinal pharmacology, *Pharmacol. Ther. 72*, 149−169.
20. Mäler, L., Blankenship, J., Rance, M., and Chazin, W. J. (2000) Site-site communication in the EF-hand Ca^{2+}-binding protein calbindin D_{9k}, *Nature 7*, 245−250.
21. Heredia, V. V., Thomson, J., Nettleton, D., and Sun, S. (2006) Glucose-induced conformational changes in glucokinase mediate allosteric regulation: Transient kinetic analysis, *Biochemistry 45*, 7553−7562.
22. Rostovtseva, T. K., Liu, T.-T., Colombini, M., Parsegian, V. A., and Bezrukov, S. M. (2000) Positive cooperativity without domains or subunits in a monomeric membrane channel, *Proc. Natl. Acad. Sci. U.S.A. 97*, 7819−7822.
23. Monod, J., Wyman, J., and Changeux, J. P. (1965) On the nature of allosteric transitions: a plausible model, *J. Mol. Biol. 12*, 88−118.
24. Kay, L. E. (1998) Protein dynamics from NMR, *Nat. Struct. Biol. 5*, 513−517.
25. Kern, D., and Zuiderweg, E. R. P. (2003) The role of dynamics in allosteric regulation, *Curr. Opin. Struct. Biol. 13*, 748−757.
26. Fraser, R. A., Duncan, W. J., and Collar, A. R. (1965) Lambda-Matrices and Canonical Forms, in *Elementary Matrices and Some Applications to Dynamics and Differential Equations*, Chapter 3, Cambridge University Press, Cambridge, England.

BI700030R